Characterization of tin oxides by x-ray-photoemission spectroscopy

Jean-Marc Themlin*
Laboratoire de Spectroscopie Moléculaire de Surface, Institute for Studies in Interface Sciences, Facultés Universitaires Notre Dame de la Paix, 61 rue de Bruxelles, B-5000 Namur, Belgium

Mohammed Chtaïb†
Laboratoire Interdisciplinaire de Spectroscopie Electronique, Institute for Studies in Interface Sciences, Facultés Universitaires Notre Dame de la Paix, 61 rue de Bruxelles, B-5000 Namur, Belgium

Luc Henrard and Philippe Lambin
Laboratoire de Physique du Solide, Institute for Studies in Interface Sciences, Facultés Universitaires Notre Dame de la Paix, 61 rue de Bruxelles, B-5000 Namur, Belgium

Jacques Darville and Jean-Marie Gilles
Laboratoire de Spectroscopie Moléculaire de Surface, Institute for Studies in Interface Sciences, Facultés Universitaires Notre Dame de la Paix, 61 rue de Bruxelles, B-5000 Namur, Belgium
(Received 12 May 1991; revised manuscript received 25 February 1992)

Using well-defined samples of SnO and SnO_2, we have focused our attention on the way the two tin oxides could be distinguished using x-ray-photoemission spectroscopy (XPS). Polycrystalline SnO, oxidized in air to give SnO_2, sputtered by argon-ion bombardment to give SnO and single-crystalline SnO_2 have been examined using XPS in order to study the formal valencies of tin in these partly ionic compounds. On the basis of a tin $3d$-level line-shape analysis, we show that a sizable chemical shift of 0.7 ± 0.05 eV exists between (formal) Sn^{4+} and Sn^{2+}. Using a least-squares fitting routine, we are able to follow the evolution of both ionic species upon argon-ion bombardment. This evolution shows up more strongly in the valence-band region, where SnO is characterized by an additional structure attributed to Sn $5s$–derived levels. Our experimental results are interpreted using calculated tight-binding bulk densities of states. Finally, we propose a procedure for the quantitative evaluation, by XPS, of the relative concentration of the two oxides.

I. INTRODUCTION

It has long been recognized that the formal valencies of tin in its oxidized forms cannot be distinguished using XPS, this technique being usually used for estimating the [Sn]/[O] ratio. This conclusion has been reached because, in order to avoid energy scale calibration procedures, the energy difference between the O $1s$ and the Sn $3d$ lines had been used[1] as a possible index of the oxidation stage, but had failed to indicate any chemical-shift difference between the two tin oxides. According to Lau and Wertheim,[1] the change in free-ion potential between Sn^{2+} and Sn^{4+} is cancelled by the change in Madelung potential at tin sites between the two lattices. Other attempts[2,3] showed that a chemical shift of the order of 0.5 eV does exist between the Sn $3d$ locations in the two oxides. Nevertheless, in spite of being a time-consuming procedure, the best way to distinguish between SnO and SnO_2 seems to be detailed analysis of their different valence-band (VB) regions, as have been demonstrated by Lau and Wertheim[1] and recently by Sherwood.[4] One purpose of this paper is to investigate how this could be used in order to yield meaningful quantitative values of the relative concentrations of Sn^{2+} and Sn^{4+} species in a given sample.

However, most of these past studies were realized on poorly defined powders,[3] electrochemically oxidized metallic samples,[2] or an air-oxidized and sputtered metallic tin[4] that suffered from uncertainties with respect to the actual composition. We have recently shown[5] that a thick layer of good-quality SnO_2 covers air-oxidized SnO. Sputtering with 500-eV argon ions reduces a layer of roughly 35 Å thick, thereby inducing a $Sn^{4+}\rightarrow Sn^{2+}$ transformation. In this work, we are able to remove the oxidized layer completely by sputtering with more energetic ($E_P=4500$ eV) argon ions. This procedure leaving "pure" SnO, we avoid energy calibration procedures by directly comparing SnO_2 (before sputtering) and SnO spectra on the same sample. For the sake of comparison, spectra from SnO_2 single-crystalline samples will also be presented. Furthermore, in our extensive UPS study[5] of polycrystalline black SnO, we could resolve the (formal) Sn^{4+} and Sn^{2+} components of the Sn $4d$ levels (binding energy $E_B\approx26$ eV with respect to E_F). We are thus able to study samples with a well-defined surface composition and in excellent condition for comparing SnO and SnO_2

spectra in the Sn 3*d*, Sn 4*d*, and VB regions. Since this study was made using a standard XPS spectrometer, it is also interesting to verify whether or not a direct decomposition procedure of the Sn 3*d* levels can still be efficient in spite of the lower available resolving power.

This paper is organized as follows. By extension of our work on Sn 4*d* bands observed with UPS, we apply the same strategy to the intense XPS Sn 3*d* levels, to ascertain the surface concentration in Sn^{4+}, Sn^{2+}, or Sn^{0} species. Then we present the corresponding Sn 4*d* and valence-band spectra, which show significant differences when compared to existing results.[4] The relevant features of the VB spectra, which reflect the very different chemical bonding mechanisms in the two oxides, are interpreted in terms of theoretical bulk densities of states (DOS) from the band-structure calculations of Munnix and Schmeits[6] (for SnO_2) and Themlin *et al.*[5] (for SnO). Finally, we point out the qualitative differences useful to identify the most abundant oxide within the XPS sampling depth and we show how the VB and near-core spectra can be used to facilitate quantitative evaluations based on detailed Sn 3*d* level line-shape analysis.

II. EXPERIMENT

The tin dioxide single crystals were grown in our laboratory by the reactive vapor phase transport method introduced by Helbig.[7] The perfect aspect of the single-crystalline platelets cut from hollow needles oriented along the *c* axis allowed us to study the (110) face without any polishing. Further details about the SnO_2 single crystals are given elsewhere.[8] Since the thermal instability of stannous oxide precludes the growth of single crystals,[9] we have pressed pure (99.9%) SnO powder into pellets at high pressure. It is known that SnO readily oxidizes in air at room temperature,[1] and we have shown[5] that one could use this oxidized layer as a good quality SnO_2. For SnO_2 single crystals as well as for oxidized SnO, only a slight argon-ion bombardment ($E_P=4500$ eV, current density of roughly 5 $\mu A/cm^2$ for 1 min) was used to remove a small amount of carbon contamination as well as a hydrated layer. The degree of cleanliness was assessed by the absence of the C 1*s* line and the lack of the hydroxyl-characteristic tail usually observed in the O 1*s* levels.

In order to observe "pure" SnO, higher doses of argon ions ($E_P=4500$ eV, current density of roughly 5 $\mu A/cm^2$) were used to sputter away the top SnO_2 layer. The actual sputtering time necessary to remove the covering layer completely was longer after the SnO pellet had been exposed to ambient air for an extended period before its introduction into the spectrometer. The decrease of the Sn^{4+} concentration was detected in our XPS spectra using a Sn 3*d* level line-shape analysis and monitored several times during the preparation procedure. The latter was stopped as soon as the Sn^{4+} component was reduced to a negligible level. We therefore avoided the growth of an Sn^{0} component, which arises only for larger sputtering times, following the reduction of black SnO.

The XPS data have been recorded with a Surface Science Instruments SSX-100 spectrometer that uses a monochromatized Al $K\alpha$ x-ray source ($h\nu=1486.6$ eV). The overall resolution of the spectrometer was 0.4 eV. The base pressure during the measurements was in the low 10^{-10}-mbar range. A differentially pumped ion gun operated at 4.5 keV was used for argon-ion sputtering. Charging effects were important on unsputtered SnO_2 (either on single crystals or on air-oxidized SnO) and were neutralized using a flood gun operated at 2 eV kinetic energy. By inspecting the valence-band structures, care was taken that the small binding energy shifts of the core levels were not resulting from a charging effect. The spectra are referenced to the Fermi level of a gold-plated metal in electrical contact with the oxide sample.

III. RESULTS AND DISCUSSION

The Sn 3*d* levels

The Sn 3*d* core-level spectra recorded on air-oxidized SnO and on SnO_2 single crystals look very similar. In contrast, the Sn 3*d* spectrum of sputtered SnO appears slightly shifted (by ≈ 0.7 eV) toward low binding energies (E_B). The observed spin-orbit splitting of 8.4 eV is in good agreement with the tabulated value.[10] We will interpret the shift of E_B for SnO as a true chemical shift, and we postulate that this shift is due to the appearance of a Sn^{2+} component. The origin of our interpretation arises from our recent analysis of Sn 4*d* UPS spectra obtained when sputtering similar samples,[5] which led to the appearance and growth of a Sn^{2+} component situated at 0.65 eV toward lower E_B. We believe that the same situation shows up in the present Sn 3*d* spectra and is easier to detect since the large spin-orbit splitting allows the fit of a single Voigt profile per component. Since a physically significant fit requires that the number of parameters be a minimum, we have fixed the position of the Sn^{4+} component at 486.3 eV, the binding energy for which we expect Sn^{4+} ions to be dominant in SnO_2 on SnO. The Sn^{2+} component is dominant in the SnO spectrum and the best fit suggests a location at 0.73 eV from the Sn^{4+} component toward lower E_B. A Sn^{0} component separated by 2.5 eV from the Sn^{4+} component was generally necessary to account for the small bump on the low-E_B side of the SnO spectra. This is consistent with our previous studies which show that in contrast to what happens with SnO_2 (Ref. 8), a prolonged sputtering of SnO leads to the creation of metallic tin.[5]

The consistency of our fit was checked by monitoring $3d_{5/2}$ levels several times during the sputtering. Figure 1 clearly demonstrates the growth of the Sn^{2+} component and the gradual disappearance of the Sn^{4+} component upon sputtering. The parameters used for the fits are given in Table I. It appears that the effect of argon-ion bombardment is not a mere reduction of the top SnO_2 layer following oxygen preferential sputtering, but that the underlying black SnO becomes progressively uncovered. Indeed, we have found that it was not possible to reach such a high degree of reduction by applying the same treatment on well-characterized SnO_2 single crystals, which undergo a limited reduction (see Sec. V). In this latter case, one rather observes the alteration of the

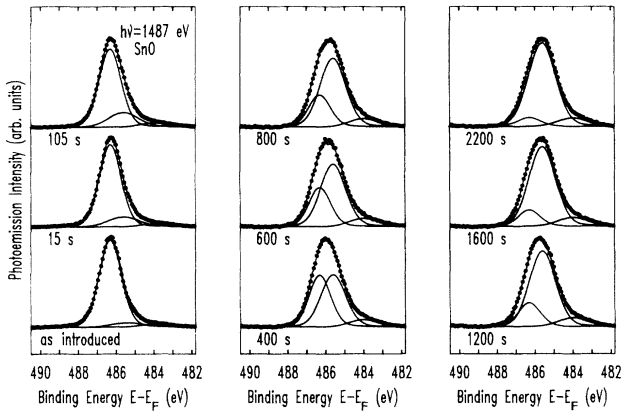

FIG. 1. XPS spectra of Sn $3d_{5/2}$ measured at increasing argon-ion (E_P=4.5 keV) sputtering time on air-oxidized SnO (circles) until the complete removal of the covering SnO_2 layer. The spectra have been normalized to equal height and the background due to inelastically scattered electrons has been subtracted. The solid curves, labelled by the etching time, are the result of a curve fitting into three components. The solid line closest to the raw-data points is the sum of the individual components.

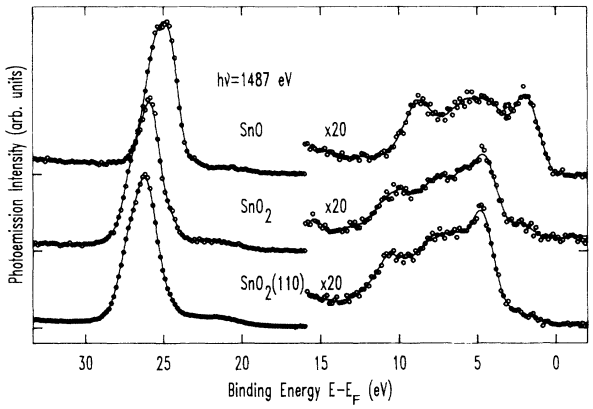

FIG. 2. XPS spectra of valence-band and near-core region of air-oxidized SnO (middle curve labeled SnO_2), sputtered SnO (top curve), and SnO_2 single crystals [SnO_2 (110), bottom curve]. The solid line represents smoothed data, and the binding-energy scale refers to the Fermi level. The VB region has been magnified with respect to the Sn 4*d* region on which the data have been normalized.

rutile electronic structure SnO_{2-x} inherent to a high-oxygen-vacancy concentration. We therefore assume that the final spectra are characteristic of the quadratic lattice of SnO, and not of a high-vacancy rutile-structured SnO_{2-x} phase. The appearance of a Sn^0 component for longer sputtering times further confirms this view, since the ratio of the partial sputtering yields $Y(O)/Y(Sn)$ in SnO_2 prevents the creation of metallic tin for the rutile phase.[8,11] It should be stressed here that the energy difference between O 1*s* and Sn 3*d* levels amounts to 48.77 eV for SnO_2 and 48.68 eV for SnO. As recalled in the Introduction, a measurement only of the relative chemical shift between the two oxides it thus clearly insufficient for identification purposes.

The valence-band and Sn 4*d* core region

Figure 2 shows the valence-band and near-core region of SnO_2 (110), air-oxidized SnO, and sputtered SnO. Once more, the close similarity of the two characteristic curves of SnO_2 confirms the good quality of the SnO_2 layer on top of SnO. The most notable difference between the two oxides is in the presence of a prominent peak characteristic of SnO, at the lower-E_B side of the VB. We have proposed a tin 5*s*-derived origin for this peak in our earlier UPS[5] study of SnO. These Sn 5*s*-derived levels, which in SnO_2 form the bottom of the conduction band, become part of the occupied VB in SnO, in order to accommodate the additional electrons located on tin cations. The observation of a resonant enhancement that occurs at the Sn 4*d* absorption threshold has confirmed the tin-derived origin of this peak.[5]

The first, most prominent peak of SnO at low E_B is not merely due to a shift of the O 2*p*-derived peak which is the leading peak of SnO_2. Indeed, one can clearly see in Fig. 3 the gradual appearance of the Sn 5*s*-derived structure at low E_B. The spectra are given for increasing sputtering times corresponding to selected spectra of Fig. 1. The O 2*p*-derived structure at E_B=4.5 eV keeps the

TABLE I. Parameters used in the fits to the Sn 3*d* spectra of Fig. 1. The binding energies were fixed at 486.3 eV for the Sn^{4+} component and 485.6 eV for the Sn^{2+} component, and both components share a Gaussian-to-Lorentzian mixing ratio of 0.87.

	Sn^{4+}		Sn^{2+}		Sn^0	
Sputtering time (s)	Height (arb. units)	FWHM (eV)	Height (arb. units)	FWHM (meV)	Height (arb. units)	FWHM (meV)
As introduced	954	1.373	48	1.9	30	1.8
15 s	906	1.343	110	1.9	30	1.8
105 s	861	1.364	162	1.834	45	1.8
400 s	568	1.340	575	1.524	80	1.8
600 s	431	1.336	690	1.550	90	1.8
800 s	353	1.346	759	1.581	90	1.8
1200 s	264	1.358	830	1.611	100	1.8
1600 s	181	1.350	877	1.640	100	1.8
2200 s	98	1.451	924	1.680	100	1.8

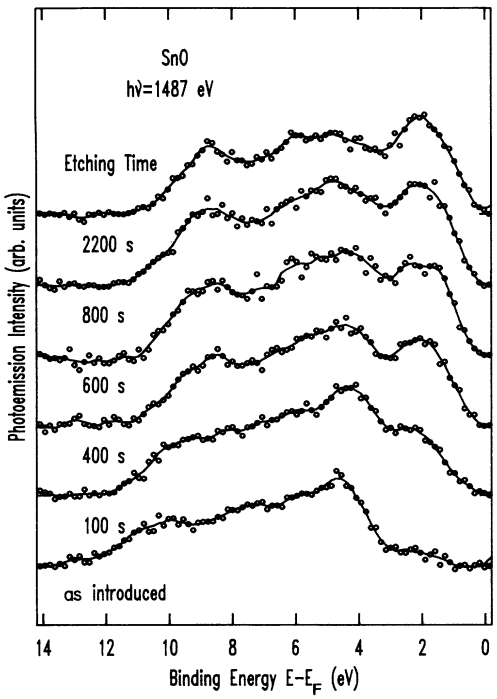

FIG. 3. Set of valence-band XPS spectra at selected sputtering times corresponding to Fig. 1. The growth of the Sn 5*s*-derived structure as the underlying SnO becomes progressively uncovered can clearly be seen. The solid line represents smoothed data. The spectra have been normalized to equal height.

same location and becomes buried with increasing sputtering time. It is worth mentioning here that the lack of significant energy shift for these VB structures rules out the possibility of appreciable band-bending variations upon sputtering and justifies our interpretation of the Sn 3*d* binding-energy shift in terms of a chemical shift. As we have suggested previously,[5] the intensity ratio I(Sn 5*s*)/I(O 2*p*) can be used to monitor the gradual evolution

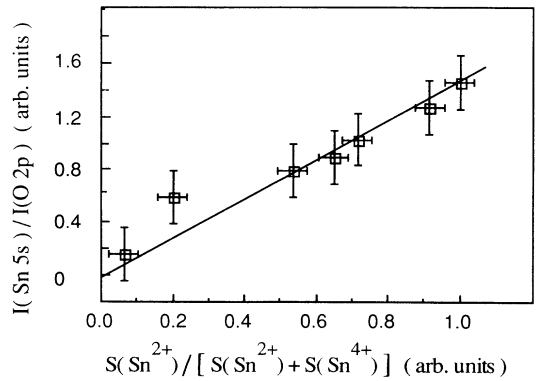

FIG. 4. Relation between experimental intensity ratio I(Sn 5*s*)/I(O 2*p*) (measured from Fig. 3) and the area ratio $S(Sn^{2+})/[S(Sn^{4+})+S(Sn^{2+})]$ (or equivalently the relative Sn^{2+} concentration) during the sputtering of the SnO_2 layer on top of SnO. The latter quantity is derived from the Sn 3*d* line-shape analysis of the XPS spectra (from Fig. 1).

TABLE II. Binding-energy difference between Sn 4*d* levels and the leading peak of the valence band. The Sn $4d_{5/2}$ level was used in UPS. The leading peak of the SnO valence band in UPS is the O 2*p*-derived structure. The value in parentheses for UPS has been measured using the Sn 5*s*-derived shoulder.

	UPS	XPS[a]	XPS (This work)
SnO_2	21.1 eV	21.1 eV	21.5 eV
SnO	20.5 eV (22.4 eV)	23.7 eV	23.1 eV

[a]Reference 4.

of the sputtered layer toward the SnO stoichiometry. Figure 4 emphasizes the relation between the I(Sn 5*s*)/I(O 2*p*) ratio and the area ratio $S(Sn^{2+})/[S(Sn^{4+})+S(Sn^{2+})]$ determined from our Sn 3*d* fit. The quantity $S(Sn^{2+})/[S(Sn^{4+})+S(Sn^{2+})]$ approximates $[Sn^{2+}]/([Sn^{2+}]+[Sn^{4+}])$, the relative concentration of Sn^{2+} species in the sampled layer.

Another important feature is the energy separation of the Sn 4*d* peak from the most prominent (leading) peak of the valence band. When going from the low photon energies characteristic of the UPS regime to x rays, the ratio of the partial photoionization cross sections, σ(Sn 5*s*)/σ(O 2*p*), taken from tabulated values undergoes a sixfold magnification.[5] The Sn 5*s*-derived structure accordingly grows in XPS above the O 2*p* peak, while it remains a shoulder in UPS spectra. Since the prominent peak at the low-E_B side of the XPS VB of the two oxides has two different origins, their energy separation with the Sn 4*d* peak position is higher than in UPS. We give these energy separations in Table II, together with the corresponding UPS values as well as other XPS values.[4] For similar sample preparations, we obtain higher energy separations in XPS than in UPS, because we have used the position of the Sn $4d_{5/2}$ level in the better resolved UPS spectra. In XPS, the partly resolved doublet shows up as a single broad peak, and this broadening shifts the location of the peak toward higher E_B. As judged from our previous results,[5] such a broadening can account for shifts as large as 0.7 eV and should be greater for SnO where the doublet is more resolved. The energy differences measured in this work are 21.5 and 23.1(5) eV for SnO_2 and SnO. Although they differ by only 1.6(5) eV as compared with the 2.6 eV value reported by Sherwood,[4] they can be used to distinguish SnO_2 from SnO qualitatively. The origin of the discrepancies with the results of Ref. 4 will be further discussed below.

IV. INTERPRETATION USING TIGHT-BINDING CALCULATIONS

We show in Fig. 5 the XPS spectra of the valence band of SnO_2 and SnO obtained at high resolution and for a sufficiently high counting time. The background due to inelastically scattered electrons has been subtracted. The origin of the binding-energy scale has been chosen at the valence-band maximum of the theoretical simulations to

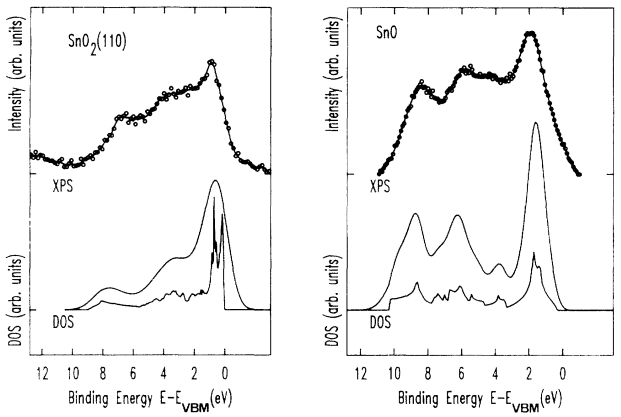

FIG. 5. Experimental valence-band XPS spectra of SnO_2 (110) (left part), and of SnO (right part) compared with simulated spectra (lower curves). The unbroadened bulk DOS (Ref. 12 for SnO_2 and Ref. 5 for SnO) weighted by the partial photoionization cross sections at 1487 eV are also shown. They have been convoluted with a Lorentzian Gaussian (87% Gaussian character) to yield the simulated spectra.

be described below, on which the experimental spectra were arbitrarily aligned. Indeed, in order to interpret our measurements, we have generated synthetic spectra starting from the available theoretical results. The synthetic spectrum of SnO_2 was generated from the orbital-resolved partial density of states[12] (DOS) of Munnix and Schmeits. Starting from the work of Robertson[13] based on the tight-binding method, they had modified the parameter set of an empirical tight-binding (TB) Hamiltonian to describe the electron states in the solid.[6] The width of the theoretical VBDOS was adjusted to fit the width of the early UPS data of Gobby.[14] Since then, we have shown that this width (9 eV) was overestimated, as we have deduced a VB width of 7.5 eV from our UPS spectra.[8] The bottom, sharp spectrum of Fig. 5 (left part) has been obtained from the sum of the above-mentioned orbital-resolved DOS, weighted by the corresponding partial photoionization cross sections.[15] The convoluted result is also presented in Fig. 5, where it accounts for the finite lifetime and instrumental resolution broadenings.

The gradual sputtering of the oxidized SnO_2 layer upon argon-ion bombardment induces the appearance and growth of the Sn $5s$-derived structure in the VB, while the remainder of the VB suffers small changes. It is interesting to see if the O $2p$-derived structure is still present at the high-E_B side of the Sn $5s$ structure characteristic of SnO. Concerning tin monoxide, the experimental spectrum has been obtained on a heavily sputtered sample kept at a temperature of 500 K during ion bombardment. The Sn $3d$ line-shape analysis reveals that most of the tin ions are in the formal valence state Sn^{2+} while the preparation procedure leaves the reduced layer completely free of metallic Sn^0. The synthetic spectrum was generated as described above, using our own orbital-resolved DOS.[5] The VBDOS have also been derived using a tight-binding method where the SnO VB width measured in UPS[5] has been used as an experimental input. The effect of the Madelung potential at tin and oxygen sites has been taken into account to fix the relative positions of the Sn $5s$ and O $2p$ atomic levels that are the starting point of the TB calculations. The parameters were further refined to fit the XPS spectra, which is more characteristic of the bulk electronic structure than the UPS spectra owing to the larger photoelectron escape depth. Four structures can actually be found in the XPS VB spectrum of SnO, the most prominent one being mainly derived from Sn $5s$ levels (60%) hybridized with O $2p$ levels. The small bump around $E_B=4$ eV due to the O $2p$-derived levels could well be distinguished. The structures around $E_B=2$ eV and $E_B=9$ eV originate from antibonding and bonding Sn $5s$–O $2p$ states, respectively.

Our XPS VB shape compares favorably with the results of Lau and Wertheim,[1] but is rather different from Sherwood's.[4] This reflects probably the different ways of producing well-defined samples. In our work and that of Lau and Wertheim,[1] the SnO_2 sample is a single crystal. As far as SnO is concerned, Lau and Wertheim have identified the result of the vacuum decomposition of SnO_2 at high temperature on a gold substrate as being red SnO, using ion backscattering and Mössbauer experiments. Although our calculation is based on the structure of black SnO, we believe that the main features of the VB are determined by the actual valence state of the cations, the details being modulated by the crystallographic structure. The situation may be less favorable in Sherwood's study where oxidized, metallic tin samples were used, the heavily air-oxidized sample being taken as SnO_2. The SnO was produced by argon-ion etching of the SnO_2-covered tin surface until some underlying metal was seen. One problem is that, as stated by these authors, the spectrum has some contribution from metal. Moreover, this does not signify that the underlying metal is reached, since metallic tin can easily be produced by etching SnO (Ref. 16). It is likely that an underlying SnO_2 layer still contributes to the experimental spectrum, since our experience[16] with sputtering SnO_2 single crystals at $E_P=4.5$ keV suggests that it is not possible to obtain the complete oxide reduction $SnO_2 \rightarrow SnO$. Indeed, the XPS spectrum of SnO in Ref. 4 is strikingly similar to our own XPS spectra of SnO_2. The Sn $4d$ XPS spectra are not shown in Sherwood's study, but it is likely that they may still have important Sn^{4+} contribution. Since the latter lies at 0.7 eV toward higher E_B, and taking into account the lower resolving power used in Sherwood's experiment, this would explain the larger separation between the Sn $4d$ location and the VB leading peak. Another point worth mentioning here is that we were able to reproduce fairly well the VB structures of both SnO and SnO_2 without including any Sn $4d$ contribution. Since this level is situated at a higher E_B around 26 eV, we believe it is too far away from the shallower ionic levels to hybridize appreciably with them.

V. QUANTITATIVE ESTIMATES OF SnO AND SnO_2 CONCENTRATIONS

The comparison between the overall VB of the two oxides reveals the gross differences that can be useful for

identification purposes. Apart from the obvious difference in the number of structures (three for SnO_2 and four for SnO) which could require long counting time to be revealed, other differences that can be clearly seen in Fig. 5 are (i) the apparent VB width (in the current resolution and experimental conditions of this work: 10.4 eV for SnO_2 and 12 eV for SnO), (ii) the sharper character of the VB structures of SnO, in particular the two peaks around $E_B=6$ and 9 eV, characteristic of this layered compound, due to the longer photohole lifetime with respect to SnO_2, (iii) the presence of a local minimum to the high energy side of the first (leading) peak of the VB (Sn 5*s*-derived) for SnO.

These qualitative differences should provide the basis for a preliminary rapid identification of the most abundant oxide within the XPS sampling depth (see Fig. 3). A useful step in this identification procedure is the easy determination of the energy difference between the Sn 4*d* peak and the first peak in the VB toward low E_B (the first one is often the most prominent, at least if one oxide is dominant). As shown in the preceding section, one finds 21.5 eV for SnO_2 and 23.1(5) eV for SnO. For the intermediate cases, which should often be met in practice, the height of the Sn 5*s* peak with respect to the O 2*p* peak will serve as a visual indication of the amount of SnO present. The ratio of the peak intensities $[I(\text{Sn } 5s)/I(\text{O } 2p)]$ could be used in a subsequent step to infer an approximate concentration ratio using Fig. 4. This approximate determination of the $[Sn^{2+}]/([Sn^{2+}]+[Sn^{4+}])$ concentration ratio should ease the quantitative fit of the Sn $3d_{5/2}$ levels, in terms of two components separated by 0.73 eV, even without an absolute binding-energy calibration. When some metallic tin is present in the surface layer, a third component should be considered. However, this does not bring a real difficulty since this contribution is clearly separated (see Fig. 1) from the two others, 2.5 eV away from the Sn^{4+} component.

This procedure has been applied to the study of the reduction of the $SnO_2(110)$ face upon argon-ion bombardment. The sputtering of single-crystalline $SnO_2(110)$ leads essentially to the same effect as the one observed during the sputtering of polycrystalline SnO_2 on top of SnO. In the VB region, a structure develops at low E_B, in the band gap of SnO_2. However, its intensity rapidly saturates with increasing sputtering time. Figure 6 (lower part) reveals the XPS spectrum of SnO_2 (110) valence band at saturation. From a rapid comparison with the spectra displayed in Fig. 3, one can infer that the SnO concentration at saturation is in the range of 30–40 %, which will be confirmed by the following detailed analysis. A mean value of 0.54 for the intensity ratio $I(\text{Sn } 5s)/I(\text{O } 2p)$ has been determined from the VB spectrum of three freshly introduced SnO_2 single crystals. We have previously suggested[8] that (i) the oxygen deficiency in the sputtered layer induces the change of the cation oxidation state from Sn^{4+} to Sn^{2+}, creating local SnO-like chemical environment, and (ii) the band-gap defect states originate from Sn 5*s*-derived levels. If this is true, we should be able to see a Sn^{2+} component in the Sn 3*d* spectrum. Using the value of 0.54 in conjunction with Fig. 4, we expect

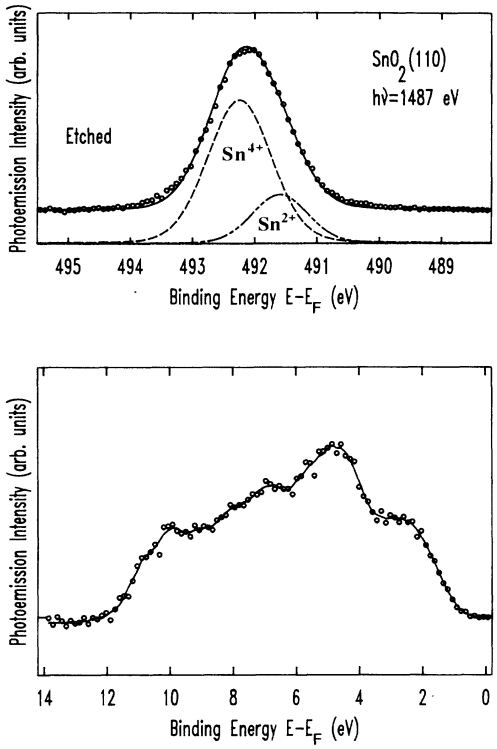

FIG. 6. XPS valence-band spectrum of sputtered SnO_2 (110) (lower curve). The sputtering time has been chosen so that further increase of the ion dose does not increase the height of the Sn 5*s*-derived feature. The upper curve represents the corresponding Sn $3d_{5/2}$ levels experimental spectrum (dots) and the result of the fit (solid line) in terms of two components Sn^{4+} and Sn^{2+}.

an area ratio $S(Sn^{2+})/[S(Sn^{4+})+S(Sn^{2+})]$ of 0.38. Figure 6 (upper part) shows the result of the best fit obtained from the Sn $3d_{5/2}$ levels. The area ratio $S(Sn^{2+})/[S(Sn^{4+})+S(Sn^{2+})]=0.32$ is in good agreement with the predicted value as judged from the VB spectrum. It thus seems possible, for instance, to fix *a priori* some plausible limits on the intensity or area ratio between the two components, which should ease the fitting procedure of the Sn 3*d* spectrum. The area ratio $S(Sn^{2+})/[S(Sn^{4+})+S(Sn^{2+})]$ of 0.32 suggest that only 32% of the sputtered layer is effectively reduced into SnO. Further experimental work aimed at comparing sputtering effects in SnO and SnO_2 is currently underway.[16]

VI. CONCLUSIONS

Using well-defined samples of SnO and SnO_2, we have investigated the capability of XPS to discriminate between stannic and stannous oxides. The SnO_2 which covers the air-oxidized SnO was sputtered with 4.5 keV argon ions, completely exposing the black SnO. The gradual shift of the Sn 3*d* levels toward low E_B in the XPS spectra during the completion of the procedure is interpreted as due to the growth of a Sn^{2+} component (and the disappearance of the Sn^{4+} component) as the underlying

SnO becomes progressively uncovered.

In the VB region, a Sn 5*s*-derived structure grows at low E_B and becomes the most prominent peak as the sputtering proceeds. Neither knowledge of only the chemical shift, which amounts to 0.73 eV, nor the use of absolute binding energies described in this work could suffice in practice to discriminate with certainty between the two oxides. We propose therefore to use the intensity ratio $I(\text{Sn } 5s)/I(\text{O } 2p)$ derived from VB spectra in order to estimate *a priori* the concentration ratio $[Sn^{2+}]/([Sn^{2+}]+[Sn^{4+}])$.

The comparison of our XPS results with simulated theoretical spectra derived from tight-binding calculations emphasizes some important differences between the VB XPS spectra of the two tin oxides. The VB of SnO, with a larger width of about 12 eV, is actually made of four structures, since the O 2*p*-derived levels near $E_B = 4$ eV are still visible. Furthermore, the sharper character of the VB structures and the existence of a localized minimum to the high-E_B side of the leading peak suggests the possibility of quickly identifying SnO if it is dominant in the sampled layer. The SnO_2 VB has a smaller apparent width (10.4 eV) and is made of three broader structures. The two oxides could also be identified by the simple measurement of the energy difference between Sn 4*d* and the leading peak of the VB [21.5 eV for SnO_2 and 23.1(5) eV for SnO]. In order to bring quantitative results, the identification procedure involves a Sn 3*d* fitting procedure. The latter should be eased by the *a priori* knowledge of the approximate area ratio $S(Sn^{2+})/[S(Sn^{4+})+S(Sn^{2+})]$ as derived from the VB region [the ratio $I(\text{Sn } 5s)/I(\text{O } 2p)$]. The study of the reduction of single crystalline SnO_2 (110) upon sputtering demonstrates the feasibility of the proposed procedure. It also confirms in a direct way the close relation between defect band-gap states and near-surface Sn^{2+} species.

ACKNOWLEDGMENTS

This work was supported by the Belgian National Fund for Scientific Research (FNRS), the Belgian Ministry for Science Policy (SPPS) through IRIS concerted actions, and the interuniversity Research Project in Interface Sciences (PAIT-ISIS). One of us (Ph.L.) thanks the Belgian National Fund for Scientific Research for financial support. We are grateful to Professor R. Caudano who made the SSX-100 spectrometer available to us, to Toan Le Quoc and Marc Vermeersch for their assistance during the measurements, and to Dr. M. Schmeits for communicating unpublished results.

*Present address: Groupe de Physique des Etats Condensés, Faculté des Sciences de Luminy, Case 901 (Université d'Aix-Marseille II), F-13288 Marseille, CEDEX 9, France.

†Present address: Laborlux S. A., 1 avenue des Terres Rouges, L-4004 Esch-sur-Alzette, Luxembourg.

[1]C. L. Lau and G. K. Wertheim, J. Vac. Sci. Technol. **15**, 622 (1978).

[2]R. O. Ansell, T. Dickinson, A. F. Povey, and P. M. A. Sherwood, J. Electrochem. Soc. **124**, 1360 (1977).

[3]E. Paparazzo, G. Fierro, G. M. Ingo, and N. Zachetti, Surf. Interface Anal. **12**, 438 (1988).

[4]P. M. A. Sherwood, Phys. Rev. B **41**, 10 151 (1990).

[5]J.-M. Themlin, P. Lambin, J. Darville, J.-M. Gilles, and R. L. Johnson (unpublished).

[6]S. Munnix and M. Schmeits, Phys. Rev. B **27**, 7624 (1983).

[7]B. Thiel and R. Helbig, J. Cryst. Growth **32**, 259 (1976).

[8]J.-M. Themlin, R. Sporken, J. Darville, R. Caudano, J.-M. Gilles, and R. L. Johnson, Phys. Rev. B **42**, 11 914 (1990).

[9]P. Buck, in *Preparation and Crystal Growth of Materials with Layered Structures,* edited by R. M. A. Lieth (Reidel, Dordrecht, 1977).

[10]J. C. Fuggle and M. Mårtensson, J. Electron Spectrosc. Relat. Phenom. **21**, 275 (1980).

[11]J.-M. Themlin, Ph.D. thesis, Facultés Universitaires Notre-Dame de la Paix, Namur, 1991.

[12]M. Schmeits (private communication).

[13]J. Robertson, Phys. Rev. B **28**, 3378 (1983).

[14]P. L. Gobby and G. J. Lapeyre, in *Physics of Semiconductors: Proceedings of the 13th International Conference, Rome, 1976,* edited by F. G. Fumi (North-Holland, Amsterdam, 1976), p. 150.

[15]J. J. Yeh and I. Lindau, At. Data Nucl. Data Tables **32**, 1 (1985).

[16]J.-M. Themlin (unpublished).